# Dynamically Manipulating Topological Physics and Edge Modes in a Single Degenerate Optical Cavity

Xiang-Fa Zhou, Xi-Wang Luo, Su Wang, Guang-Can Guo, Xingxiang Zhou, Han Pu, and Zheng-Wei Zhou

Phys. Rev. Lett. **118**, 083603 — Published 22 February 2017

DOI: 10.1103/PhysRevLett.118.083603

# Dynamically manipulating topological physics and edge modes in a single degenerate optical cavity

Xiang-Fa Zhou[1,2],Xi-Wang Luo[1,2],Su Wang[1,2],Guang-Can Guo[1,2],Xingxiang Zhou[1,2],Han Pu[3,4],Zheng-Wei Zhou[1,2]*
[1] *Key Laboratory of Quantum Information, Chinese Academy of Sciences, University of Science and Technology of China, Hefei, 230026, China*
[2] *Synergetic Innovation Center of Quantum Information and Quantum Physics, University of Science and Technology of China, Hefei, 230026, China*
[3] *Department of Physics and Astronomy, and Rice Center for Quantum Materials, Rice University, Houston, TX 77251, USA*
[4] *Center for Cold Atom Physics, Chinese Academy of Sciences, Wuhan 430071, P. R. China*

We propose a scheme to simulate topological physics within a single degenerate cavity, whose modes are mapped to lattice sites. A crucial ingredient of the scheme is to construct a sharp boundary so that open boundary condition can be implemented for this effective lattice system. In doing so, the topological properties of the system can manifest themselves on the edge states, which can be probed from the spectrum of output cavity field. We demonstrate this with two examples: a static Su-Schrieffer-Heeger chain and a periodically driven Floquet topological insulator. Our work opens up new avenues to explore exotic photonic topological phases inside a single optical cavity.

PACS numbers: 42.50.Pq, 03.65.Vf, 42.50.Tx, 64.60.Ht

*Introduction* — Exploration of topological physics has become one of the most fascinating frontiers in recent years [1–3]. Since Haldane and Raghu proposed to transcribe the topological features of electronic models into photonic ones [1–5], studies on topological photonics have been widely developed [6–19]. Although there is no concept of band filling due to the abscence of Pauli exclusion principle, bulk-edge correspondence is still present in this linear bosonic system [7–10]. In such systems, detection of the topologically edge modes are regarded as one of the most important and direct methods of probing their topological properties [9, 11, 14, 17, 18, 20–26].

Recent studies show that the internal degrees of freedom of quantum systems [27–33] may be used as synthetic dimensions, which lead to the reduction of physical resources. In the context of photonics, it has been shown [33, 34] that synthetic gauge fields in a two-dimensional (2D) system can be effectively simulated by using a 1D array of degenerate cavities [35–37], where the internal degenerate cavity modes serve as an extra dimension. However, making identical cavities to form the array is extremely challenging in practice. Hence it is highly desirable that topological phases can be simulated using just a single cavity. Furthermore, how to control the cavity decay and to construct the desired boundary condition for photons are highly nontrivial tasks.

The main purpose of the present work is three-fold: First, we show that it is indeed possible to simulate certain topological phases inside a single cavity. Second, we propose a way to construct a sharp boundary, with which edge states will emerge when the system enters the topological regime. Finally, exploiting the high controllability of the system, we show how a Floquet topological insulator can be generated by periodically modulating the cavity system. This allows us to investigate Floquet topological phases which possess many unique features not present in static systems [38–45] and a further understanding of the system [10, 14, 39, 40, 46, 47].

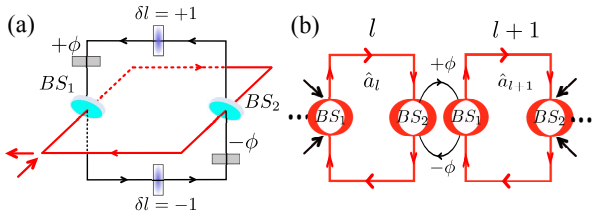


FIG. 1: (Color online). (a) Illustration of experiment setup about the degenerate cavity. (b) The effective photonic circuit of (a). $\phi$ is the imbalanced phase between the two arms of the auxiliary cavity.

*Effective 1D chain in a single cavity* — Figure 1(a) illustrates schematically the cavity system we will be working with. It contains a main cavity (horizontally oriented in the figure) which supports Laguerre-Gaussian (LG) modes with different orbital angular momenta (OAM), and an auxiliary cavity (vertically oriented in the figure) which is connected to the main cavity by two beam splitters ($BS_1$ and $BS_2$). The electric field of the LG mode, $E_l^p$, is characterized by the radial and the azimuthal quantum numbers $p$ and $l$, respectively. It is possible to make the resonance frequency of the modes to be all degenerate, i.e., independent of $p$ and $l$ (for details, see Ref. [33, 34]). For our purpose, the radial quantum number $p$ is irrelevant, and we shall neglect it henceforth. The azimuthal index $l$ characterizes the OAM of the photon, and the hopping between different OAM modes is accomplished with the aid of the spatial light modulators (SLMs) in the auxiliary cavity, which changes the OAM (i.e., the azimuthal index $l$) of the photon by $\pm\delta l$. Denote the annihilation operator for mode $l$ as $a_l$, different OAM modes are thus mapped to a 1D lattice chain, and the

hopping between them is descried by $a_l^\dagger a_{l+\delta l} + h.c.$ in the lattice model. In general, arbitrary long-range hopping can be realized by adjusting $\delta l$. The hopping strength is determined by the transmission/reflection coefficients of the beam splitters and can be further controlled by the phase retarders $\pm\phi$ [34]. The effective lattice system with nearest-neighbor hopping is schematically illustrated in Fig. 1. Note that the effective lattice size can be doubled if we take into account that a given $l$-mode comes with two orthogonal polarizations (see below).

*Creating sharp boundary* — To realize open boundaries for the effective lattice system, we would like the cavity to have an OAM cutoff $L_m$, such that modes with $l = 0$, 1, ..., $L_m$ have negligible decay rates whereas all other modes are not supported. The $l = 0$ LG mode is the usual Gaussian mode with intensity peaks at the center, whereas $l \neq 0$ LG modes all have doughnut shape whose intensities peak at a circle with radius scaled as $\sqrt{l}$. This spatial intensity distribution and the finite size of the cavity mirrors may lead to $l$-dependent decay rate. Such soft boundary due to the $\sqrt{l}$ scaling can cause serious loss of photons with large $l$ [34] and destroy all interesting physics related to edge modes (see Fig. 4(c)).

To create a sharp boundary, we take advantage of the fact that the $l = 0$ mode can be easily distinguished from the $l \neq 0$ modes and modify the cavity system as schematically shown in Fig. 2(a). Here we put two SLMs in the main cavity with $\delta l = \pm L_m$, respectively. For photons traveling in the main cavity in the direction as shown by the arrows, their OAM will change when passing the SLMs. Specifically, a photon with azimuthal index $l$ to the left of the SLMs will change it to $l - L_m$ when traveling to the right of the SLMs. Hence the mode in the main cavity becomes composite and we label this mode pair $[l, l - L_m]$ as $|l\rangle$. We make the two SLMs in the auxiliary cavity to have $\delta l = \pm(L_m + 1)$, respectively. Finally a hole is made in each of the two beam splitters connecting the main and the auxiliary cavities. The hole size is carefully designed so that, ideally, a photon with $l = 0$ will always go through the hole without being reflected, while all other modes with $l \neq 0$ will be reflected with certain probability. It is not difficult to see that [34], with this design, (1) a composite mode $|0\rangle$ in the main cavity may hop to $|1\rangle$, but not to $|-1\rangle$; (2) a composite mode $|L_m\rangle$ may hop to $|L_m - 1\rangle$, but not to $|L_m + 1\rangle$; (3) a composite mode $|l\rangle$ with $0 < l < L_m$ may hop to either $|l - 1\rangle$ or $|l + 1\rangle$. In other words, we have succeeded in creating two sharp boundaries such that only composite modes $|l = 0, 1, \cdots, L_m\rangle$ can exist in the main cavity.

It is clear that the key here is the design of the hole in the beam splitters which should let $l = 0$ mode pass through with high probability, while not affecting too much the $l \neq 0$ modes. The sharpness of the boundary is then determined by how well we can distinguish $l = 0$ photon from $l \neq 0$ modes. We can achieve good distinguishability due to the small intensity overlap between

*Realizing and probing SSH model* — Our first example concerns the realization of the Su-Schrieffer-Heeger

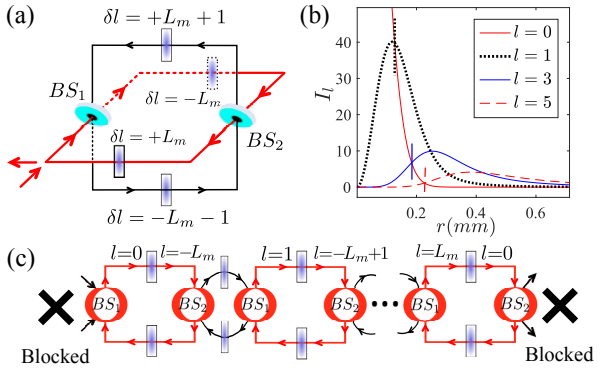


FIG. 2: (Color online) (a) Proposed experimental setup of single degenerate cavity to simulate 1D finite lattice using composite modes induced by two SLMs with $\delta l = \pm L_m$. Two hollow beam splitters are employed so that only modes $l = 0$ can transmit through the hole. (c) is the effective photonic circuit of (a). (b) Normalized intensity profiles $I_l(r) = |E_l(r)|^2$ for different $l$-modes calculated using the parameters discussed in [34]. The vertical lines indicate the possible center pinhole sizes in each BS for different hopping steps $n = 1$, 3, and 5, with the corresponding fraction of $l = 0$ photon intensity inside the pinhole as 78%, 96%, and 99%, respectively.

$l = 0$ mode with the adjacent $l = \pm 1$ modes. Experimentally, sharper boundaries can be obtained for larger hopping step $n$ if we replace the two SLMs in the auxiliary cavity with $\delta l = \pm(L_m + n)$. In this way, the effective lattice sites are represented by modes $|l = 0, n, \cdots, nL_m\rangle$. We need only to distinguish $l = 0$ mode from $l = \pm n$ modes whose intensity overlap scales as $e^{-n}$ (see Fig. 2(b) and details in [34]).

With the creation of sharp boundaries, we can now use it to explore the topological properties of the system. We will use two examples below to demonstrate this.

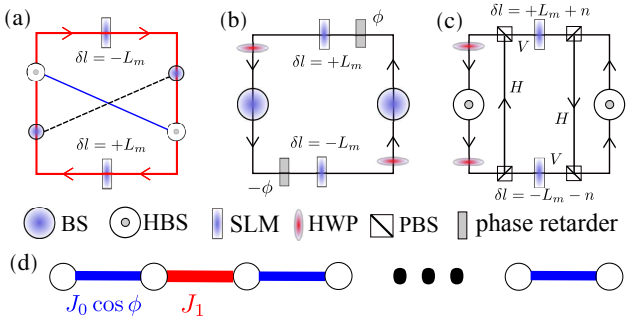


FIG. 3: (Color online) Schematic diagram of simulating 1D SSH chain. (a) shows the skeleton inside of the main cavity with two-auxiliary-cavity circuits depicted in (b) and (c), where optical circuits related to the hopping $J_0 \cos\phi$ and $J_1$ are shown. (d) is the diagrammatic representation of the Hamiltonian $H$. BS: beam splitter. HBS: BS with a pinhole in the center. SLM: spatial light modulator. HWP: half-wave plate. PBS: polarization beam splitter which transmit vertical polarized photons and reflect horizontal polarized photons.

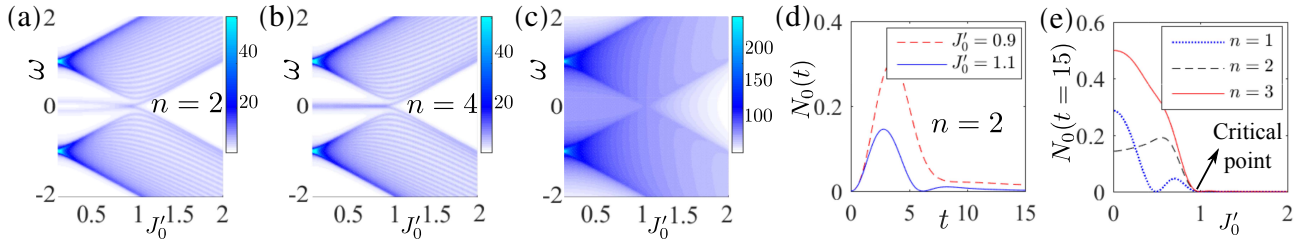


FIG. 4: (Color online) (a) and (b) show the spectrum $\tau(\omega)$ of model (1) for $J_1 = 1$ and $L_m = 49$ with the decay rates $\gamma_j = 0.05(1 + e^{-j/\sqrt{25}} + e^{-|j-L_m|/\sqrt{25}})$ for $n = 2$ and $n = 4$ respectively, where the influence of $H'$ in remaining lattices is also taken into account. (c) shows the output spectrum of a prolonged chain using the same decay as in (a), which corresponds to the soft boundary condition discussed in the context. (d) shows the dynamics of $N_0$ with hopping step $n = 2$ for an input pulse $a(t)_{in,0} = \exp[-(t-3)^2/8]/\sqrt{2\sqrt{\pi}}$ at site $j = 0$ with the decay given in (a) for fixed $J_0' = 0.9$ and 1.1 respectively. (e) plots the amplitude $N_0$ for different $n$ at $t = 15$ along with $J_0'$, which drops to zero across the phase transition point.

(SSH) model [48], a prototypical 1D topological model, as schematically illustrated in Fig. 3. Here we take advantage of the fact that each OAM mode $l$ comes with two orthogonal polarizations, which we will map to lattice sites as $E_{l,H} \to 2l$ and $E_{l,V} \to 2l+1$. The coupling between modes $a_{2l}$ and $a_{2l+1}$ can be easily accomplished with polarization rotators inside the auxiliary cavities. The coupling $a_{2l+1} \leftrightarrow a_{2l+2}$ corresponds to a polarization-dependent hopping $E_{l,V} \leftrightarrow E_{l+1,H}$, which can be realized with the combination of the polarized beam splitters (PBSs) and the SLMs (See Fig.3(c) and [34] for details). The total effective Hamiltonian simulated can then be written as $H_T = H + H'$ with

$$H = \sum_{l=0}^{L_m} \left[ J_0 \cos(\phi) a_{2l}^\dagger a_{2l+1} + J_1 \alpha_{l+1}^{(n)} a_{2l+1}^\dagger a_{2l+2} + h.c. \right], \quad (1)$$

where $H$ is the desired SSH model Hamiltonian when $\alpha_{l+1}^{(n)} = 1$. $H'$ describes the interaction of other cavity modes in the remaining lattice sites, whose explicit form can be found in [34]. The phase dependent coupling proportional to $\cos\phi$ is due to the interference effect inside the auxiliary cavity, which can be used as a convenient control knob to adjust the hopping amplitude $J_0' \equiv J_0 \cos\phi$ [34]. The presence of pinhole results in a reduction of coupling strength at the lattice site $2(l+1)$ defined by $\alpha_{l+1}^{(n)} = 1 - \eta_{l+1}^{(n)}$ for giving hopping step $n$, where $\eta_{l+1}^{(n)}$ is the portion of photons for modes $|(l+1)n\rangle$ inside the pinhole of the BSs. As shown in [34], $\eta_{l+1}^{(n)}$ decreases exponentially along with $l$. In the ideal case $\alpha_{l+1}^{(n)} = 1$, the system becomes topologically nontrivial when $J_0' < J_1$. In the presence of sharp boundaries, this leads to topologically induced edge states.

To illustrate how the presence of the edge states can be detected, let us calculate the output spectrum of the cavity using the Langevin equations [33, 49]

$$\partial_t a_j = -i[a_j, H(t)] - \frac{\gamma_j}{2} a_j - \sqrt{\gamma_j} a_{in,j}\,, \quad (2)$$

with $\gamma_j$ the decay rate on lattice site $j$. The output field is linked to the dynamics inside the cavity through the standard input-output relation $a_{out,j}(t) = a_{in,j}(t) + \sqrt{\gamma_j} a_j(t)$. In the frequency domain, this leads to $a_{out,j}(\omega) = \sum_{j'} (\delta_{jj'} - T_{jj'}) a_{in,j'}(\omega)$ with the transmission element $T_{jj'} = -i\langle j|\sqrt{\Gamma}[\omega - H + i\Gamma/2]^{-1}\sqrt{\Gamma}|j'\rangle$ and the decay matrix $\Gamma = \mathrm{diag}\{\gamma_0, \cdots, \gamma_{Lm}\}$.

Figure 4(a) and (b) show the total transmission rate $\tau(\omega) = \sum_{j,j'} |T_{jj'}|^2$ as functions of $J_0'$ for $n = 2$ and 4 respectively. The imperfection induced by the pinhole in the BSs results in site-dependent hoppings characterised by $\alpha_{l+1}^{(n)}$ and unwanted coupling $|0\rangle \to |-n\rangle$ and $|L_m\rangle \to |L_m + n\rangle$ at boundaries [34], both of which are explicitly taken into account. For $n = 2$, the presence of such unwanted tunneling couples bilateral edge modes in the topological nontrivial regime. This results in the splitting of edge modes into two branches around $\omega = 0$ [34]. For larger hopping step $n = 4$, the two branches merge as such hopping decreases exponentially with $n$. For comparison, we plot the transmission rate for a soft boundary in Fig. 4(c), where the presence of edge modes is completely erased. This clearly demonstrates the importance of constructing the sharp boundary in our system. Figure 4(d) illustrates the dynamics of $N_0 = \langle a_0^\dagger a_0 \rangle$, the amplitude of the first site for $n = 2$, when initially we inject an input pulse from this site. In the topological regime $J_0'/J_1 < 1$, due to the presence of the edge state, $N_0$ persists over a very long time; whereas in the non-topological regime when $J_0'/J_1 > 1$, $N_0$ decays to zero rather quickly. In Fig. 4(e), we plot the value of $N_0$ at $t = 15$ as a function of $J_0'$ when $J_1$ is fix to be 1 for different $n$. A transition at $J_0'/J_1 = 1$ can be easily seen, which can be viewed as a clear evidence of the topological phase transition at that critical point [34]. We note that the oscillation shown for small hopping step is due to the interference of two split edge modes in the presence of unwanted hopping at boundaries. For larger $n$, such oscillatory behavior disappears.

*Floquet topological insulator and edge modes inside cavity* — In the second example, we take advantage of the flexibility of our cavity system and also investigate

a periodically driven situation. Such Floquet systems have received great attention recently as they exhibit many unique properties absent in the static models [41–45]. We periodically modulate the system by modulating the phase delay as $\phi(t) = \phi_0 + \alpha\cos(\Omega t/2)$, which leads to a periodic modulation of the hopping amplitude $J_0' = J_0\cos\phi$. When $\phi_0 = 0$, we have $\cos[\alpha\sin(\Omega t/2)] = j_0(\alpha)+2j_2(\alpha)\cos(\Omega t)+...$ with $j_n(x)$ the $n$th order Bessel function. We can choose $\alpha$ such that all high-order terms can be safely neglected. This leads to a Floquet version of Hamiltonian (1) where the hopping $J_0\cos\phi$ is now replaced with the modified one as $J_0 + \lambda\cos(2\pi t/T)$ with $T = 2\pi/\Omega$. Experimentally, such high frequency phase modulation of $\phi$ can be implemented with the aid of an electro-optic modulator, where the modulation frequency can be as high as tens of GHz. This is much larger than the typical cavity coupling strength (a few MHz), and is sufficient for our purpose.

The properties of such periodic driven system can be obtained using the standard Floquet theory [34, 38–40, 46, 47]. The quasi-energies $\epsilon_q$ and Floquet modes can be solved in the composite Floquet space $T\otimes R$ where $R$ represents the usual Hilbert space and $T$ is spanned by the periodic functions $\langle t|m\rangle = e^{im\Omega t}$ [34]. The index $m$ describes the number of phonons and defines the subspace named as the $m$th Floquet replica. The wave function in the usual Hilbert space $|\psi\rangle = \sum_{m,j} c_{m,j}(t)\exp(im\Omega t)|j\rangle$ can be rewritten as $|\psi^F\rangle = \sum_{m,j} c_{m,j}(t)|m,j\rangle$, which satisfies the modified Schrödinger equation [38]

$$\frac{d|\psi^F\rangle}{dt} = -i\mathbb{H}_F|\psi^F\rangle - \frac{\gamma}{2}|\psi^F\rangle\,, \tag{3}$$

with the last term describing the dissipation effect. The time-independent Floquet Hamiltonian reads $\mathbb{H}_F = \hat{F}_m\otimes\hat{H}^{(m)} + \Omega\hat{F}_z\otimes I_R$, where $I_R$ is the identity operator in $R$-space, $H(t) = \sum_m \hat{H}^{(m)}e^{im\Omega t}$, $(F_m)_{i,j} = \delta_{j,i+m}$, and $(F_z)_{m,n} = m\Omega\delta_{m,n}$.

For high driving frequency $\Omega$, different Floquet bands are almost uncoupled. When $\Omega$ decreases, the interaction of Floquet replicas for $m = 0$ and $m = \pm1$ leads to the appearance of gaps at $\pm\Omega/2$ . Topological transition occurs when bands in different replicas start to overlap with each other, and is signalled by the presence of edge states at quasi-energy $\epsilon_q = 0$ and $\Omega/2$, respectively.

As in the previous example, the presence of the Floquet phase transition and the associated edge states can be observed by detecting the total output spectrum defined as $T(\omega) = \sum_{\psi^F(0)}\sum_{m,j}|c_{m,j}(\omega)|^2$ for $\omega\in(-\Omega/2,\Omega/2)$ [34]. The input state $\psi^F(0)$ can be prepared by feeding the cavity using mode $j$ with different frequency $\omega = m\Omega$. When $\omega$ is resonant with the Floquet modes, it induces a peak in the spectrum. Especially around $\omega = 0$ or $\Omega/2$, $T(\omega)$ is almost completely determined by the presence of the mid-gapped edge modes, while contributions from other modes are greatly reduced. This provides a direct evidence of the Floquet topological phase transitions.

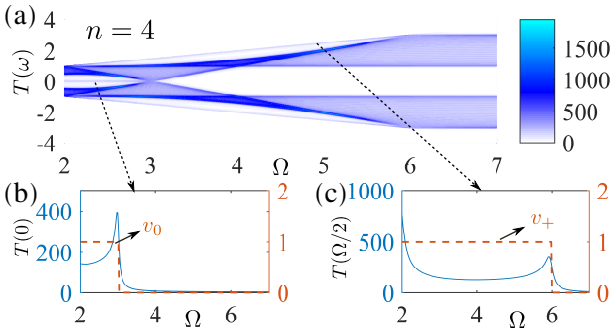


FIG. 5: (Color online). (a) The spectrum $T(\omega)$ within the Floquet zone $(-\Omega/2,\Omega/2)$ for different $\Omega$ for hopping step $n = 4$ with the same decay used in Fig. 4. Other parameters are $[J_0, J_1, \lambda] = [2, 1, 0, 1.6]$ and $L_m = 49$. (b) and (c) show the spectra $T(0)$ and $T(\Omega/2)$ along with $\Omega$, where topological transition is manifested by jumps around the phase transition points. $v_0$ and $v_+$ are their corresponding numbers of edge modes defined in [34].

Figure 5 shows the cavity output spectrum as a function of $\Omega$ within the Floquet zone, where the size effect of pinhole in the BSs is also involved. The presence of the Floquet gaps is revealed by the vanishing $T(\omega)$ around quasi-energy 0 and $\Omega/2$. In addition, starting with a topologically trivial phase at large $\Omega$, Floquet topological phase transitions occur when two replicas touch each other as $\Omega$ decreases. The construction of boundaries enable us to detect such transitions by observing the output spectrum directly. As shown in Fig. 5(b) and (c), due to the presence of finite gaps, the amplitude of $T(0)$ and $T(\Omega/2)$ exhibit staircase-like structure and jump around the critical point where the phase transition occurs. This can be viewed as a direct evidence of Floquet topological phase transitions.

*Outlook and Conclusion* — We have proposed a scheme to simulate topological physics in a single optical cavity by constructing sharp boundaries in the synthetic dimensions. All the operations about the photonic OAM modes proposed here can be reliably implemented through linear elements, which make the system experimental friendly and resource undemanding. The proposed scheme can also be extended to explore nontrivial topological physics in high dimensional system [50, 51]. In view of current experimental progress on synthetic magnetic field for photons [19] and the strong light-atom coupling inside a multimode resonator [52], effective photon-photon interactions in degenerate cavity regime [53–55] also becomes possible. Therefore our work also opens up an avenue to explore various exotic topological photonic states in optical cavity system.

*Acknowledgement* — XFZ thanks Jin-Shi Xu for helpful discussions. The authors thank the anonymous referees for many valuable suggestions. This work was funded by National Natural Science Foundation of China (Grant

Nos. 11574294, 61490711, 11474266), the Major Research plan of the NSFC (Grant No. 91536219), and the "Strategic Priority Research Program(B)" of the Chinese Academy of Sciences (Grant No. XDB01030200). HP is supported by the US NSF (Grant No. PHY-1505590) and the Welch Foundation (Grant No. C-1669).

* Electronic address: zwzhou@ustc.edu.cn[1,2]

[1] C. Nayak, S. H. Simon, A. Stern, M. Freedman, and S. D. Sarma, Reviews of Modern Physics **80**, 1083 (2008).
[2] M. Z. Hasan and C. L. Kane, Reviews of Modern Physics **82**, 3045 (2010).
[3] X.-L. Qi and S.-C. Zhang, Reviews of Modern Physics **83**, 1057 (2011).
[4] F. Haldane and S. Raghu, Phys. Rev. lett. **100**, 013904 (2008).
[5] S. Raghu and F. Haldane, Phys. Rev. A **78**, 033834 (2008).
[6] J. D. Joannopoulos, S. G. Johnson, J. N. Winn, and R. D. Meade, *Photonic crystals: molding the flow of light* (Princeton university press, 2011).
[7] Z. Wang, Y. Chong, J. D. Joannopoulos, and M. Soljačić, Phys. Rev.Lett. **100**, 013905 (2008).
[8] Z. Wang, Y. Chong, J. Joannopoulos, and M. Soljačić, Nature **461**, 772 (2009).
[9] M. Hafezi, E. A. Demler, M. D. Lukin, and J. M. Taylor, Nature Physics **7**, 907 (2011).
[10] K. Fang, Z. Yu, and S. Fan, Nature Photonics **6**, 782 (2012).
[11] A. B. Khanikaev, S. H. Mousavi, W.-K. Tse, M. Kargarian, A. H. MacDonald, and G. Shvets, Nature Materials **12**, 233 (2013).
[12] L. Lu, L. Fu, J. D. Joannopoulos, and M. Soljačić, Nature Photonics **7**, 294 (2013).
[13] Y. E. Kraus, Y. Lahini, Z. Ringel, M. Verbin, and O. Zilberberg, Phys. Rev. Lett. **109**, 106402 (2012).
[14] M. C. Rechtsman, J. M. Zeuner, Y. Plotnik, Y. Lumer, D. Podolsky, F. Dreisow, S. Nolte, M. Segev, and A. Szameit, Nature **496**, 196 (2013).
[15] M. Hafezi, S. Mittal, J. Fan, A. Migdall, and J. Taylor, Nature Photonics **7**, 1001 (2013).
[16] L. Lu, J. D. Joannopoulos, and M. Soljačić, Nature Photonics **8**, 821 (2014).
[17] W.-J. Chen, S.-J. Jiang, X.-D. Chen, B. Zhu, L. Zhou, J.-W. Dong, and C. Chan, Nature Communications **5**, 5782 (2014).
[18] L. Lu, Z. Wang, D. Ye, L. Ran, L. Fu, J. D. Joannopoulos, and M. Soljačić, Science **349**, 622 (2015).
[19] N. Schine, A. Ryou, A. Gromov, A. Sommer, and J. Simon, Nature **534**, 671 (2016).
[20] G. Liang and Y. Chong, Phys. Rev. Lett. **110**, 203904 (2013).
[21] R. Umucalılar and I. Carusotto, Phys. Rev. A **84**, 043804 (2011).
[22] S. A. Skirlo, L. Lu, and M. Soljačić, Phys. Rev. Lett. **113**, 113904 (2014).
[23] S. Mittal, J. Fan, S. Faez, A. Migdall, J. Taylor, and M. Hafezi, Phys. Rev. Lett. **113**, 087403 (2014).
[24] W. Hu, J. C. Pillay, K. Wu, M. Pasek, P. P. Shum, and Y. D. Chong, Phys. Rev. X **5**, 011012 (2015).
[25] W. Gao, M. Lawrence, B. Yang, F. Liu, F. Fang, B. Béri, J. Li, and S. Zhang, Phys. Rev. Lett. **114**, 037402 (2015).
[26] M. Hafezi, Phys. Rev. Lett. **112**, 210405 (2014).
[27] A. Celi, P. Massignan, J. Ruseckas, N. Goldman, I. B. Spielman, G. Juzeliūnas, and M. Lewenstein, Phys. Rev. Lett. **112**, 043001 (2014).
[28] H. M. Price, O. Zilberberg, T. Ozawa, I. Carusotto, and N. Goldman, Phys. Rev. Lett. **115**, 195303 (2015).
[29] T.-S. Zeng, C. Wang, and H. Zhai, Phys. Rev. Lett. **115**, 095302 (2015).
[30] F. Mei, J.-B. You, D.-W. Zhang, X. C. Yang, R. Fazio, S.-L. Zhu, and L. C. Kwek, Phys. Rev. A **90**, 063638 (2014).
[31] A. M. Yao and M. J. Padgett, Advances in Optics and Photonics **3**, 161 (2011).
[32] H. M. Price, T. Ozawa, and N. Goldman, arXiv preprint arXiv:1605.09310 (2016).
[33] X.-W. Luo, X. Zhou, C.-F. Li, J.-S. Xu, G.-C. Guo, and Z.-W. Zhou, Nature Communications **6**, 7704 (2015).
[34] See Supplimental Material for explicit introduction of degenerated cavity, the reduction of hopping amplitudes due to the pinhole, and calculation details about Floquet topological system, which includes Ref. [33, 35–40].
[35] J. Arnaud, Applied optics **8**, 189 (1969).
[36] S. A. Collins, JOSA **60**, 1168 (1970).
[37] N. Hodgson and H. Weber, *Laser Resonators and Beam Propagation: Fundamentals, Advanced Concepts, Applications*, Vol. 108 (Springer, 2005).
[38] T. Levante, M. Baldus, B. Meier, and R. Ernst, Molecular Physics **86**, 1195 (1995).
[39] J. Asbóth, B. Tarasinski, and P. Delplace, Phys. Rev. B **90**, 125143 (2014).
[40] V. Dal Lago, M. Atala, and L. F. Torres, Phys. Rev. A **92**, 023624 (2015).
[41] T. Oka and H. Aoki, Phys. Rev. B **79**, 081406 (2009).
[42] T. Kitagawa, E. Berg, M. Rudner, and E. Demler, Phys. Rev. B **82**, 235114 (2010).
[43] N. H. Lindner, G. Refael, and V. Galitski, Nature Physics **7**, 490 (2011).
[44] J. Cayssol, B. Dóra, F. Simon, and R. Moessner, physica status solidi (RRL)-Rapid Research Letters **7**, 101 (2013).
[45] A. Gómez-León and G. Platero, Phys. Rev. Lett. **110**, 200403 (2013).
[46] M. Pasek and Y. Chong, Phys. Rev. B **89**, 075113 (2014).
[47] D. Leykam, M. C. Rechtsman, and Y. D. Chong, Phys. Rev. Lett. **117**, 013902 (2016).
[48] W.-P. Su, J. Schrieffer, and A. Heeger, Phys. Rev. B **22**, 2099 (1980).
[49] D. F. Walls and G. J. Milburn, *Quantum optics* (Springer Science & Business Media, 2007).
[50] P. Harper, Proceedings of the Physical Society. Section A **68**, 874 (1955).
[51] S. Aubry and G. Andr, Israel Phys. Soc. **3**, 133 (1980).
[52] A. J. Kollár, A. T. Papageorge, V. D. Vaidya, Y. Guo, J. Keeling, and B. L. Lev, arXiv preprint arXiv:1606.04127 (2016).
[53] H. Schmidt and A. Imamoglu, Optics letters **21**, 1936 (1996).
[54] A. Imamolu, H. Schmidt, G. Woods, and M. Deutsch, Phys. Rev. Lett. **79**, 1467 (1997).
[55] S. Harris and Y. Yamamoto, Phys. Rev. Lett. **81**, 3611 (1998).